Co-operation of electricity and natural gas systems including electric vehicles and variable renewable energy sources based on a continuous-time model approach

Co-operation of Electricity and Natural Gas Systems including Electric Vehicles and Variable Renewable Energy Sources based on a Continuous-time Model Approach

Ahmad Nikoobakht[1], Jamshid Aghaei[2], Miadreza Shafie-khah[3], João P. S. Catalão[4,*]

[1]Department of Electrical Engineering, Higher Education Center of Eghlid, Eghlid, Iran

[2]Department of Electrical and Electronics Engineering, Shiraz University of Technology, Shiraz, Iran

[3]School of Technology and Innovations, University of Vaasa, 65200 Vaasa, Finland

[4]Faculty of Engineering of University of Porto and INESC TEC, Porto, Portugal

[*]***Corresponding Author*: *catalao@fe.up.pt***

Abstract: This paper proposes a stochastic framework to augment the integration of variable renewable energy sources (VRESs) in power system scheduling. In this way, the fast-response capability of gas-fired generator units (GFGUs) and vehicle-to-grid (V2G) capability of electric vehicles (EVs) can play important roles in large-scale integration of VRESs. However, the growth of GFGUs utilization can increase the grade of interdependency between power and natural gas systems. In this condition, the power system tends to demand more reliability and flexibility from the natural gas system, which creates new challenges in power system scheduling. The likely significant growth of EVs can solve this challenge and reduce the correlation between power and natural gas systems, bringing new opportunities for power system scheduling. However, a considerable literature in the field of operation of GFGUs and EVs has only focused on using the hourly discrete time model (HDTM). Undoubtedly, the major limitation of HDTM is its inability to handle the fast sub-hourly dispatch of GFGUs and energy storage capability of EVs. Accordingly, in this paper, this limitation has been solved by the operation of both energy systems with a continuous time model (CTM). The reliability test system with a ten-node gas transmission system has been analysed to show the effectiveness of the proposed problem.

Keywords: Vehicle-to-grid; electric vehicle; renewable energy sources; natural gas system; continuous time model.

1. Nomenclature

A. Indices

q	Index of Bernstein basis Function.
w, g, e	Index for generation units, wind farms and electric vehicles, respectively.
i, j	Index of nodes in natural gas system.
p	Index of natural gas pipeline.
n, m	Index of bus in power system.
s	Index of scenarios.
t	Index of continuous-time.
t'	Index of discrete-time.
l	Index of linear block.
$(\bullet)_{s,(\cdot)}$	Related to scenario s.
$(\bullet)_{(\cdot),t}$	Related to element $(\cdot)$ at time period t.
Ω_c	Sets of natural gas pipeline with compressor.

B. Parameters

σ_e	Operation cost of electrical vehicle.
σ_g	Operation cost of generating unit.
σ_w	Operation cost of wind energy curtailment.
$\tilde{\sigma}_g$	Cost of generating units in response to wind uncertainty.
σ_g^{su}	Startup cost of generating unit.
ρ_s	Probability of scenario s.
$P_g^{\max} / P_g^{\min}$	Max/min power generation capacity.
DT_g / UT_g	Minimum off/on time of generating unit.
$\overline{P}_{et}^c / \overline{P}_{et}^d$	Maximum power charging/discharging for electrical vehicles.
r_{et}^c / r_{et}^d	Maximum ramp rate for electric vehicles power charging/discharging.
$P_{nt} / P_{s,wt}$	Load forecasted/wind power
L_{it}^n	Non-electrical natural gas load.

$\widehat{P}_{et}^{c}$	The electrical vehicles operating in charging mode.
λ_e	The percentage of electric vehicles that are operating in storage mode.
B_{nm}	Susceptance of transmission line *k*.
$P_k^{\max}$	Power flow limit for a transmission line.
η_e^d / η_e^c	Cycle discharge/charge efficiency of electric vehicles.
$\overline{\pi}_i$ / $\underline{\pi}_i$	Max/min gas pressure at a node.
$\underline{f}_{1,p}$ / $\overline{f}_{1,p}$	Min/max natural gas flow for the 1 th linear block.
$\underline{G}_i$ / $\overline{G}_i$	Min/max natural gas supply.
$\varphi_{1,p}, \gamma_{1,p}$	Constants in the 1 th linear block.
$E_{et}^{\min}$ / $E_{et}^{\max}$	Min/max energy storage capacity for electrical vehicles.
$\Phi_i^{\min}$ / $\Phi_i^{\max}$	Min/max storage volume.
$\Psi_i^{\min}$ / $\Psi_i^{\max}$	Min/max storage input.
$\Psi_i^{\min}$ / $\Psi_i^{\max}$	Min/max storage output.
$\dot{\Psi}_i^{\min}$ / $\dot{\Psi}_i^{\max}$	Min /max ramp rate for storage inflow.
$\dot{\Psi}_i^{\min}$ / $\dot{\Psi}_i^{\max}$	Min /max ramp rate for storage outflow.
R^{down} / R^{up}	Ramp down/up rate capacity.
$r_g^{\max}$	Maximum up/down power generation of a generator unit in response to wind uncertainty.
$B_{q,Q}^{t}$	Bernstein basis function of order Q.
$\Re_{Q_m}^{x_t}$	Bernstein polynomial operator takes a function x_t .
$C_{q_m}^{(\bullet)}$	Bernstein coefficient of $(\bullet)$.
$\vec{C}_{Q_m}^{(\bullet)}$	Vector of Bernstein coefficients $(\bullet)$.
Q	Order of Bernstein polynomial
Θ_p	Constant of natural gas pipeline.
α, β	Fuel function coefficient of natural gas generation units.

C. Variables

$P_{s,gt}$	Power generation of generator units.
$r^{u}_{s,gt}$ / $r^{d}_{s,gt}$	Upward/downward power generation in response to wind uncertainty.
$P^{d}_{s,et}$ / $P^{c}_{s,et}$	Discharging/charging power of electrical vehicles.
$P^{c\&d}_{s,et}$	The electrical vehicle operating in storage mode.
$r^{d}_{s,wt}$	Curtailment of wind energy generation.
$w_{g,t}$ / v_{gt}	Shutdown/startup binary variable for generating unit.
u_{gt}	Generating unit status indicator, 0 means off and 1 means on.
uc_{et} / ud_{et}	Electrical vehicles charging/discharging status indicator.
$\pi_{s,it}$	Gas pressure at a node.
$f_{s,pt}$	Natural gas flow at a natural gas pipeline.
$G_{s,it}$	Natural gas supply.
$\Phi_{s,it}$	Storage volume for natural gas storage.
$\overleftarrow{\Psi}_{s,it}$ / $\overrightarrow{\Psi}_{s,it}$	Natural gas storage inflow/outflow.
$L^{e}_{s,it}$	Electrical natural gas load.
$f_{\mathrm{l},spt}$	Natural gas flow at pipeline *p* for the l th linear block.
$\vartheta_{\mathrm{l},spt}$	Binary indicator for the l th linear block.
$\dot{P}_{s,gt}$	Generating unit ramp up rate.
$P_{s,kt}$	Power flow on a transmission line.
$\delta_{s,nt}$	Voltage angle at a bus.
$E_{s,et}$	State of charge for electrical vehicles.

D. Acronyms

V2G	Vehicle-to-grid.
VRERs	Variable renewable energy resources.
GFGUs	Gas-fired generator units.
EV	Electrical vehicle.

HDTM	Hourly discrete-time model.
CTM	Continuous-time model.
CP	current paper
WEG	Wind energy generation.
TEC	Total expected cost.
WEC	Wind energy curtailment.
MINLP	Mix-integer non-linear problem.
BPs	Bernstein polynomials.
NGSSCs	Natural gas system security constraints.

2. Introduction

2.1. Motivation and Aims

In recent years, the share of VRERs like, photovoltaic (PV) systems and wind energy resources , and the GFGUs in the generation portfolio of electrical power systems have significantly grown. It is expected to generate 35% and 16% of the power generation in US by VRERs and GFGUs in the horizon of 2040, respectively [1]. However, integration of the VRERs and GFGUs could impose two main challenges for electrical power system operator. First, the inherent uncertainty of VRERs together with the transmission congestion may limit their penetrations to the electric power systems. The second challenge is the ever increasing interdependencies of electric power systems and natural gas systems through increased incorporation of GFGUs. On the other hand, the GFGUs could take part in the supply side flexibilities because of their fast startup and ramping capabilities [2] to cover the variability and uncertainty of VRERs in the electrical power systems . However, in the real-time operation, there are some doubts about if the GFGUs can participate in supply side flexibilities while the delivery of the natural gas to GFGUs should take place “just-in-time” [3]. Indeed, in some cases, e.g., in the cold seasons, supplying interruptible loads including GFGUs could be very problematic [2] and [4]. Therefore, the main strategy to deal with these challenges is to use other available resources with fast-response capabilities to cover deficiency of GFGUs in power system scheduling. Under those circumstances, battery electric vehicles, abbreviated as EVs in this paper, with fast-response capabilities, i.e., fast power dispatch and fast ramping capabilities, can play a vital role to compensate variability and uncertainty of VRER [5].

This strategy has a couple of advantages:

(i) Due to the fact that almost all EVs stay parked for up to 96% time of a day, and this stay time is much longer than the necessary time to fully recharge the batteries. Thus, the EVs with V2G capability are expected to be a new player to provide fast-response ramping capability to augment variable renewable energy penetration while maintaining total operation cost of the electric power systems in an acceptable level subject to the constraints of both electric power systems and natural gas systems.

(ii) The EV batteries like energy storage systems can capture the renewable energy excess during off peak periods once the demand is low, and reduce need for utilization of GFGUs to compensate variability and uncertainty of VRER. Accordingly, the EVs with V2G capability can reduce impact of natural gas system constraints on the operation of electric power system.

In fact, the paper motivations and aims to address the following questions:

(i) Would influence natural gas system security constraints on gas consumption, wind energy curtailment and electrical generation cost?

(ii) Would influence integration of EVs in electric power system on the natural gas system operation?

(iii) Would influence time model on the co-scheduling of the integrated electric energy and natural gas systems with EVs?

Accordingly, the co-scheduling of the integrated electric energy and natural gas systems with other available resources with fast-response capabilities, e.g., large-scale of battery electric vehicles, abbreviated as EVs, should be developed while, the security considerations of both systems are taken into account.

2.2. Literature review

Recently, a considerable literature has grown up around the co-operation of electricity and natural gas transmission systems to use fast-response capability of GFGUs to compensate the intermittent output of VRESs [3], [6], [7] and [8]. The interdependent electric and natural gas systems with intermittent output of VRESs, in a short-term scheduling formwork, has been studied in [6]. A security-constrained bi-level economic dispatch model has been proposed in [8] for co-operation of electricity and natural gas systems including wind energy generation and power-to-gas technology. In [6], [7] and [3], the impacts of natural gas constraints on the utilization of GFGUs have been investigated. Besides, these references investigate the effect of uncertain VRESs on the co-operation of electricity and gas systems.

In the above mentioned research works [3], [6], [7] and [8] the effect of storage capability of EVs, as a fast-response resource, on co-optimization of electricity and natural gas systems with share of VRER has not been studied. Alternatively, extensive research has shown that there has been an increasing interest in the co-operation of EVs and VRESs, as an energy controlling strategy, to facilitate renewable energy absorption [9]. A large number of the research work have been published on V2G and energy storage capabilities of EVs [5], [10], [11], [12], [13] and [14]. These studies have indicated that V2G would widely mitigate uncertainty of VRESs, and minimize renewable energy curtailment in an economic and secure manner through means of smart charging of EVs.

Moreover, the energy storage capability of EVs can be accounted for energy controlling purposes. In the available literature, the energy storage capability of EVs has been used for different purposes such as facilitating renewable energy absorption and provision of fast-response ramping capability [12]. Indeed, the renewable energy (especially wind energy) absorption can be improved by employing stationary EVs storage to store energy during off-peak hours and release it during peak hours [12].

Nevertheless, the most studies in the fields of co-optimization of energy systems, i.e., electricity and natural gas transmission systems, or utilization of energy storage capability of EVs with (without) fast variations of VRESs have only been modelled based on the HDTM approach.

The main disadvantage of the HDTM is that this modelling approach is unable to utilize fast-response capability of resources, i.e., GFGUs and EVs, thus, the HDTM cannot well exploit the potential fast ramping capability of the GFGUs and EVs. Consequently, this approach could not follow sub-hourly variations of VRESs .

To solve this issue, in this paper, a CTM based on Bernstein polynomial functions is adopted which allows to better schedule the ramping capability of GFGUs and EVs because it provides a more accurate representation of the sub-hourly ramping needs to follow sudden sub-hourly ramping of VRESs. Similarly, the application of the CTM in the proposed problem can modify the co-operation of electricity and gas systems, and coordinate the GFGUs and EVs to have a better response to the real-time sudden changes of the VRESs and load.

Must be remembered, all the literature cited above are not successful enough in taking the continuous time nature of some actions into account, such as sub-hourly variations of VRES and its ramping needs. Undoubtedly, the operation of GFGUs with HDTM can cause natural gas scarcity, under those circumstances, the GFGUs could not appropriately coordinate with the fast ramping capability of EVs to compensate the faster variations of VRESs leading to the happenings of ramping shortages.

In [15] , studies supercapacitor energy storage systems in microgrid with a continuous time model. Similarly, in [16] proposed a novel robust sliding-mode control using nonlinear perturbation observers for wind energy conversion systems in real time method. Likewise, in [17], proposes a novel bio-inspired optimization method based on real time method. But the real time method which is used in these references is not suitable for operation problems, because this method is very complex and intractable.

As shown in Table 1, except current paper, no reference in the literature, which was published in recent years, proposes a continuous-time model for co-scheduling of the electric energy and natural gas systems with fast-response resources, i.e., GFGUs and EVs.

Must be remembered, Table 1 compares the proposed methods which has been presented in this paper with other methods in previous studies to highlight the paper contributions.

Finally, within the context above, the contributions of this work are twofold:

(i) Developing a CTM for to co-operation of fast-response resources, i.e., the GFGUs and EVs, to capture the fast response of capabilities of these resources to supply the fast ramping requirements of sub-hourly variation of VRESs.

(ii) Proposing a two-stage stochastic optimization in a continuous-time framework to coordinate electric power and natural gas systems with fast-response resources in order to enhance the absorption of VRESs under uncertainty condition.

Table 1: Taxonomy of the flexible resource options proposed in current paper (CP).

Ref	Year	EVs	GFGUs	Natural Gas Systems	Time Model	Wind Power uncertainty (stochastic method)
[18],	2017	N	Y	Y	N	N
[19]	2018	N	Y	Y	N	N
[20]	2018	N	Y	Y	N	N
[21]	2017	N	Y	Y	N	Y
[22]	2019	N	Y	Y	N	Y
[23]	2017	N	Y	Y	N	Y
[24]	2014	Y	N	N	N	Y
[25]	2019	Y	N	N	N	Y
[26]	2016	Y	N	N	N	N
[27]	2015	Y	N	N	N	N
[28]	2020	N	N	N	N	Y
CP	-	Y	Y	Y	Y	Y

Y/N denotes that the subject is/is not considered.

3. Mathematical Continuous-time Stochastic Modelling

This section, firstly the assumptions which have been considered by this study are listed then the uncertainty modelling is debated, finally, formulation of the continuous-time stochastic co-optimization of electricity and natural gas systems with share of EVs and VRESs has been proposed.

A. Assumptions

To more transparency, the fundamental assumptions in proposed model are summarized as follows:

(*i*). In this study, the wind energy generation (WEG) has been considered as the VRES.

(*ii*). For the sake of simplicity, only WEG uncertainty has been taken into account. Nevertheless, other uncertainties associated with lines'/units' availability, number of EVs in a stationery and load forecast error can be incorporated into the proposed model.

(*iii*). The stationary EVs are divided into two groups including: first group, the EVs operated just as demand (just operated in charging mode); second group, the EVs operated as energy storage facilities (operated in both charging and discharging modes).

B. Mathematical formulation

In this section, a two-stage stochastic continuous-time formulation for scheduling electrical power and natural gas systems with fast-response resources has been proposed to deal with the WEG uncertainty and variability. The proposed two-stage stochastic problem minimizes the expected operation cost (TEC) of electric power system during the scheduling period subject to constraints (2) and (3).

$$\min \left(\left(\begin{array}{l} \sum_{e} \left(\int_{T} \left(\sigma_{e} \cdot \left(P_{0,et}^{d} - P_{0,et}^{c} \right) \right) dt \right) \\ + \sum_{g} \left(\int_{T} \left(\sigma_{g} \cdot P_{0,gt} + \sigma_{g}^{su} \cdot v_{gt} \right) dt \right) \end{array} \right) + \sum_{s} \rho_{s} \left(\begin{array}{l} \sum_{w} \left(\int_{T} \left(\sigma_{w} \cdot \left(r_{s,wt}^{d} \right) \right) dt \right) + \\ \sum_{n} \left(\int_{T} \left(\tilde{\sigma}_{g} \cdot \left(r_{s,gt}^{u} + r_{s,gt}^{d} \right) \right) dt \right) \end{array} \right) \right) \tag{1}$$

The TEC (1) includes two main parts: *the first part* includes cost of continuous-time energy storage of EVs (first term) plus continuous-time generation and startup costs of generating units (second term) before the realization of the wind uncertainty. Likewise, *the second part,* which relates to after the realization of the wind uncertainty, indicates expected costs of wind energy curtailment (WEC) (first term), corrective actions provided by generator units (second and third terms). In the following will discuss continuous-time modelling of electric power and natural gas constraints.

Electric Power Constraints: In this section, the continuous-time electric power constraints for before/after the realization of the wind uncertainty have been formulated as follows:

$$P_{g}^{\min} u_{gt} \le P_{s,gt} \le P_{g}^{\max} u_{gt}, \quad \forall s,g,t \tag{2a}$$

$$-R^{down} u_{gt} \le \frac{d\dot{P}_{s,gt}}{dt} = \dot{P}_{s,gt} \le R^{up} u_{gt}, \quad \forall s,g,t \tag{2b}$$

$$\int_{t}^{t-UT_{g}+1} u_{g,t'} dt' \le UT_{g} v_{g,t} \quad \forall g,t \tag{2c}$$

$$\int_{t}^{t-DT_{g}+1} \left(1 - u_{g,t'}\right) dt' \le DT_{g} w_{g,t} \quad \forall g,t \tag{2d}$$

$$v_{g,t} - w_{g,t} = u_{g,t} - u_{g,t-1}, \quad \forall g,t \tag{2e}$$

$$\begin{aligned} &\sum_{g(n)} P_{0,gt} + \sum_{e(n)} P_{0,et}^{c\&d} + \sum_{w(n)} P_{0,wt} \\ &\quad - \sum_{k(n,m)} P_{0,kt} + \sum_{k(m,n)} P_{0,kt} = P_{nt} + (1-\lambda_{e}) \widehat{P}_{et}^{c}, \forall e,n,t \end{aligned} \tag{2f}$$

$$\begin{aligned} &\sum_{g(n)} P_{s,gt} + \sum_{e(n)} P_{s,et}^{c\&d} + \sum_{w(n)} \left(P_{s,wt} - r_{s,wt}^{d} \right) \\ &- \sum_{k(n,m)} P_{s,kt} + \sum_{k(m,n)} P_{s,kt} = P_{nt} + (1-\lambda_{e}) \widehat{P}_{et}^{c}, \forall s > 0, e,n,t \end{aligned} \tag{2g}$$

$$-P_{k}^{\max} \le P_{s,kt} = B_{nm} \cdot \left(\delta_{s,nt} - \delta_{s,mt} \right) \le P_{k}^{\max}, \forall s,n,m,k,t \tag{2h}$$

$$0 \le r_{s,wt}^{d} \le P_{s,wt}, \quad \forall s > 0, w,t \tag{2i}$$

$$P_{s,gt} = P_{0,gt} + \left(r_{s,gt}^{u} - r_{s,gt}^{d} \right), \quad \forall s,g,t \tag{2j}$$

$$0 \le r^{u}_{s,gt} / r^{d}_{s,gt} \le r^{\max}_{g}, \quad \forall s,g,t \tag{2k}$$

$$\frac{dE_{s,et}}{dt} = \eta^{c} P^{c}_{s,et} - \frac{P^{d}_{s,et}}{\eta^{d}}, \quad \forall s,e,t \tag{2l}$$

$$P^{c\&d}_{s,et} = P^{c}_{s,et} + P^{d}_{s,et}, \quad \forall s,e,t \tag{2m}$$

$$\int_{T}\left(\eta^{c} P^{c}_{s,et} + \frac{P^{d}_{s,et}}{\eta^{d}}\right) = 0, \quad \forall s,e \tag{2n}$$

$$-\overline{P}^{c}_{et}\lambda_{e} uc_{et} \le P^{c}_{s,et} \le 0, \quad \forall s,e,t \tag{2o}$$

$$0 \le P^{d}_{s,et} \le \overline{P}^{d}_{et}\lambda_{e} ud_{et}, \forall s,e,t \tag{2p}$$

$$-r^{c}_{et}\lambda_{e} uc_{et} \le \frac{dP^{c}_{s,et}}{dt} \le 0, \forall s,e,t \tag{2q}$$

$$0 \le \frac{dP^{d}_{s,et}}{dt} \le r^{u}_{et}\lambda_{e} uc_{et}, \forall s,e,t \tag{2r}$$

$$E^{\min}_{et}\lambda_{e} \le E_{s,et} \le E^{\max}_{et}\lambda_{e}, \forall s,e,t \tag{2s}$$

$$uc_{et} + ud_{et} \le 1, \forall e,t \tag{2t}$$

$$P_{s,g,t=0} = P^{0}_{g}\ , E_{s,e,t=0} = E^{0}_{e}\ ,$$

$$P^{c}_{s,e,t=0} = P^{c0}_{s,e}\ ,\ P^{d}_{s,e,t=0} = P^{d0}_{s,e} \tag{2u}$$

The lower and upper limits on power generation of generator units are enforced by (2a). Continuous-time ramp down and up rate are imposed by (2b). Constraints (2c) and (2d) enforce continuous-time minimum up/down time limits for each generator unit. Constraint (2e) indicates state of each generator unit, e.g., if $v_{g,t} = 1$ and $w_{g,t} = 0$ then unit g is turned on and vice versa. Constraints (2f) and (2g) enforce continuous-time power balance at each bus before and after the realization of the wind uncertainty, respectively.

Constraint (2h) indicates the DC power flow on a transmission line which is dependent on the voltage angle difference between the corresponding buses and the impendence of transmission line. Besides, the power flow limit for each transmission line is presented in this constraint. The WEC is limited by (2i). The power generation of generator units before and after the realization of the uncertainty is linked by (2j). The deployed up/down corrective actions of on-line generator units after the realization of the wind uncertainty is limited by (2k). The continuous-time constraints of EV storage energy are presented by (2l)–(2u). The continuous-time state of charge in the EV battery is shown by (2l). Where η^{c} / η^{d} in (2l) is charging/discharging efficiency. Constraint (2m) shows the dispatched power of EV batteries. Constraint (2n) imposes energy balance for the EV batteries per day. The limits on EV batteries charging and discharging are enforced by (2o) and (2p), respectively. The limitations on the continuous-time charging and discharging ramping rate are imposed by (2q) and (2r), respectively. Constraint (2s) represents the EV batteries capacity limit. Once the stationary EV batteries is joined to the power network, the EV batteries would be charged

or discharged, or remain in the idle mode which is presented through (2t). It should be noted that, $(1-\lambda_e)$ in constraints (2f) and (2g) shows the percentage of EVs in a stationary that just operating in charging mode. Likewise, λ_e (as a value changes between 0 and 1) in constraint (2o) – (2s) determines the percentage of EVs in a stationary that wanting participation in the day-ahead market, thus, they can operate in charging or discharging modes. The vectors of constant initial values to solve equations (2b), (2q) and (2r) are enforced by (2u).

Natural Gas Constraints: Here, the continuous-time natural gas constraints before/after the realization of the wind uncertainty have been formulated as follows:

$$\pi_{s,it} = \overline{\pi}_i \ , \quad \forall s,i,t \tag{3a}$$

$$\underline{\pi}_i \le \pi_{s,it} \le \overline{\pi}_i \ , \quad \forall s,i,t \tag{3b}$$

$$\begin{cases} \sum_{1} \left(\varphi_{1,p} \cdot f_{1,spt} + \gamma_{p,1} \cdot \vartheta_{1,spt} \right) = \Theta_p \left(\pi_{s,it} - \pi_{s,jt} \right) \\ \forall s,i,j,p,1,t \end{cases} \tag{3c}$$

$$\vartheta_{1,spt} \cdot \underline{f}_{1,p} \le f_{1,spt} \le \vartheta_{1,spt} \cdot \overline{f}_{1,p}, \forall s,p,1,t \tag{3d}$$

$$f_{s,pt} = \sum_{1} f_{1,spt}, \forall s,p,t \tag{3e}$$

$$\sum_{1} \vartheta_{1,spt} \le 1, \forall s,p,t \tag{3f}$$

$$\underline{G}_i \le G_{s,it} \le \overline{G}_i \tag{3g}$$

$$\sum_{1} \left(\varphi_{1,p} \cdot f_{1,spt} + \gamma_{p,1} \cdot \vartheta_{1,spt} \right) \ge \Theta_p \left(\pi_{sit} - \pi_{sjt} \right), \quad \forall p \in \Omega_c \quad \text{and} \quad \forall s,i,j,p,1,t \tag{3h}$$

$$f_{s,pt} \ge 0, \quad \forall p \in \Omega_c \text{ and } \forall s,p,t \tag{3i}$$

$$\pi_{s,it} \le \xi_p \pi_{s,jt}, \forall p \in \Omega_c \text{ and } \forall s,i,j,p,t \tag{3j}$$

$$\frac{d\Phi_{s,it}}{dt} = \Psi_{s,it} - \Psi_{s,it}, \forall s,i,t \tag{3k}$$

$$\Phi_i^{\min} \le \Phi_{s,it} \le \Phi_i^{\max}, \forall s,i,t \tag{3l}$$

$$\Psi_i^{\min} \le \Psi_{s,it} \le \Psi_i^{\max}, \forall s,i,t \tag{3m}$$

$$\Psi_i^{\min} \le \Psi_{s,it} \le \Psi_i^{\max}, \forall s,i,t \tag{3n}$$

$$\dot{\Psi}_i^{\min} \le \frac{d\Psi_{s,it}}{dt} \le \dot{\Psi}_i^{\max}, \forall s,i,t \tag{3o}$$

$$\dot{\Psi}_i^{\min} \le \frac{d\breve{\Psi}_{s,it}}{dt} \le \dot{\Psi}_i^{\max}, \forall s,i,t \tag{3p}$$

$$L_{s,it}^{e} = \alpha + \beta P_{s,gt}, \forall g \in \Omega_{NG} \text{ and } \forall s,i,t \tag{3q}$$

$$L_{s,it} = L_{s,it}^{e} + L_{it}^{n}, \ \forall s,i,t \tag{3r}$$

$$\breve{\Psi}_{s,it} - \hat{\Psi}_{s,it} + G_{s,it} + \sum_{p(i,j)} f_{s,pt} - \sum_{p(j,i)} f_{s,pt} = L_{s,it}, \forall s,i,t \tag{3s}$$

$$\breve{\Psi}_{s,i,t=0} = \breve{\Psi}_{s,i}^{0}, \ \hat{\Psi}_{s,i,t=0} = \hat{\Psi}_{s,i}^{0}, \quad \Phi_{s,i,t=0} = \Phi_{s,i}^{0}, \ \forall s,i,t \tag{3t}$$

The natural gas pressure at the source nodes is maximum which shows by (3a). The limits on lower and upper natural gas pressures at the demand nodes is enforced by (3b). The natural gas flow through a pipeline, i.e., $p\,(i.,j)$, without (with) compressor is modelled by the Weymouth equation, which is a nonlinear equation. So, this equation make proposed problem to a mix-integer non-linear problem (MINLP), therefore, employing a solver for solve such problem, i.e., MINLP, does not guarantee to find a global optimum solution, particularly once the problem scale is large. Hence, in order to solve this issue, in this paper a piecewise linear equation for the Weymouth equation has been used in order to harness the computational advantages of linearity [29]. Consequently, the linear Weymouth equation for pipeline without compressor is shown by (3c). In this equation, Θ_p is parameter which depends on pipeline features length, friction, natural gas compositions, diameter and temperature [1]. The minimum and maximum limit on the piecewise linear pieces are enforced by (3d). Also, the total gas flow through a pipeline is calculated by (3e). Constraint (3f) indicates that only one linear pieces must be active. Constraint (3g) enforces lower and upper limits on natural gas supply.

The gas flow in pipeline with gas compressor is specified by (3h). Constraint (3i) indicates that the pipeline with gas compressor generally has predefined gas flow direction. Also, terminal nodal pressures of pipeline with gas compressor is constrained by compressor factor as shown in (3j). The volume of natural gas storage facility is governed by (3k). The minimum and maximum limit on the volume of natural gas storage, inflow/outflow and inflow/outflow ramping routes for each natural gas storage facility are enforced by constraints (3l) – (3p), respectively. Constraint (3q) shows the electricity load, i.e., the GFGUs, which links electric power and natural gas systems. Constraint (3r) indicates total natural gas load, i.e., non-electricity load, i.e., L_{it}^{n}, plus electricity load, i.e., L_{it}^{e}. Constraint (3s) shows that the gas flow out of node i is equal to the gas flow injected to node i. The starting (initial) values for the state routes are stated in (3t) wherein $\breve{\Psi}_{s,i}^{0}$, $\hat{\Psi}_{s,i}^{0}$ and $\Phi_{s,i}^{0}$ are constant initial values of each decision variable.

4. Continuous-Time Model

Before to begin this process, different approaches have existed that can be used to address the continuous-time model of a function or a data set [30] and [31]. In this paper, the Bernstein polynomial (BP) approach, among different approaches, has been chosen to model a function or a data set in continuous-time model. Criteria for selecting the BP approach was as follows:

(i) Implement this approach is simple.

(ii) The accuracy of BP approach is adjustable.

(iii) This approach can be calculated very quickly on a computer [30].

The procedures of the BP approach are explained in detail as follows:

At first, the BP of degree Q has been defined by:

$$B_{q,Q}^{t} = \binom{Q}{q} t^{q} (1-t)^{Q-q} \tag{4a}$$

The BP of degree Q plays a vital role in the continuous-time model.

To model a function, i.e., x_t , for time period T, in continuous-time model, the following steps should be implemented:

(i) The time period T is divided into M intervals, i.e., $T_m = [t_m, t_{m+1}) \rightarrow T = \cup_{m=1}^{M} T_m$, length of each interval is $T_m = t_{m+1} - t_m$.

(ii) The BP operator $\Re_{Q_m}^{(\cdot)}$ is implemented on function x_t at each interval T_m and maps it into a Qth-order polynomial.

$$\Re_{Q_m}^{x_t} = \sum_{q_m=0}^{Q_m} C_{q_m}^{x_t} B_{q_m,Q_m}^{t-t_m}, \quad t \in [t_m, t_{m+1}) \tag{4b}$$

The equation (4b) represents the function x_t in continuous-time model. One advantage of the equation (4b) is that this equation can represent in the matrix form, the implementable of this form is simple. Thus, the matrix form of equation (4b) is presented as follows:

$$\Re_{Q_m}^{x_t} = \begin{bmatrix} C_{0_m}^{x_t} & C_{1_m}^{x_t} & \cdots & C_{Q_m}^{x_t} \end{bmatrix} \begin{bmatrix} B_{0_m,Q_m}^{t-t_m} \\ B_{1_m,Q_m}^{t-t_m} \\ \vdots \\ B_{Q_m,Q_m}^{t-t_m} \end{bmatrix} = \vec{C}_{Q_m}^{x_t} \vec{B}_{q_m,Q_m}^{t-t_m} \tag{4c}$$

Where $\vec{C}_{Q_m}^{x_t}$ is vector of Bernstein coefficients and $\vec{B}_{q_m,Q_m}^{t-t_m}$ is vector of Bernstein basis functions for $m = 1, \ldots, M$; $q_m = 0_m, \ldots, Q_m$, which are shown in Fig.1.

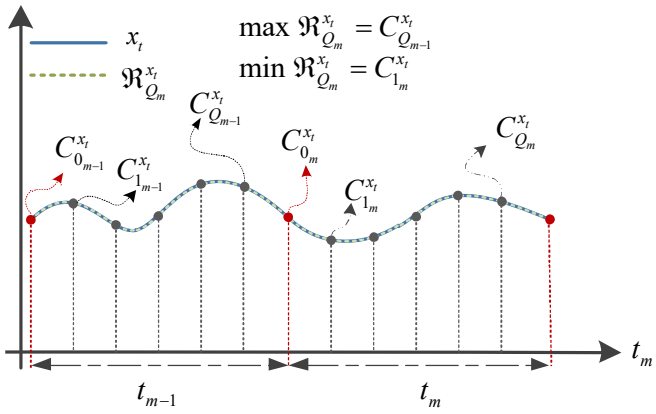

Fig.1. *The Bernstein coefficients for* x_t .

The main properties of the BP operator that are used in this paper have been addressed as follows:

(i) If the order Q_m for BP operator $\Re_{Q_m}^{x_t}$ is increased, the error approximation, for continuous time model of function x_t, reduces, which has been shown by (4d).

$$\lim_{Q_m \to \infty} \Re_{Q_m}^{x_t} = x_t \tag{4d}$$

(ii) The derivative of BP operator $\Re_{Q_m}^{x_t}$ can be represented by (4e).

$$\dot{\Re}_{(Q-1)_m}^{x_t} = Q_m \sum_{Q_m=0}^{(Q-1)_m} \left(C_{Q_m}^{x_t} - C_{(Q-1)_m}^{x_t} \right) \vec{B}_{q_m,(Q-1)_m}^{t} \tag{4e}$$

(iii) The BP operator has convex hull property, which causes that $\Re_{Q_m}^{x_t}$ and $\dot{\Re}_{(Q_m-1)}^{x_t}$ are limited between their max and min coefficients.

$$\min_{\forall q_m} \left\{ C_{q_m}^{x_t} \right\} \le \Phi_{Q_m}^{x_t} \le \max_{\forall q_m} \left\{ C_{q_m}^{x_t} \right\} \tag{4f}$$

$$\min_{\forall q_m} \left\{ \frac{C_{q_m}^{x_t} - C_{(q-1)_m}^{x_t}}{Q_m} \right\} \le \dot{\Phi}_{(Q_m-1)}^{x_t} \le \max_{\forall q_m} \left\{ \frac{C_{q_m}^{x_t} - C_{(q-1)_m}^{x_t}}{Q_m} \right\} \tag{4g}$$

This property has a pivotal role later to address max/min power generations and up/down ramp rates in continuous time model approach.

(iv) In the continuous time approach, continuity through first and end points of each interval for function x_t played an important role. Accordingly, constraint (4h) must be addressed in the proposed model.

$$C_{0_m}^{x_t} = C_{Q_{m-1}}^{x_t} \tag{4h}$$

Likewise, the derivative of $\Re_{Q_m}^{x_t}$ should also be continuous in the first and end points of each interval. So, the following constraint must be satisfied.

$$C_{1_m}^{x_t} - C_{0_m}^{x_t} = C_{Q_{m-1}}^{x_t} - C_{(Q-1)_{m-1}}^{x_t} \tag{4i}$$

These constraints are important component in the continuous time model approach, and plays a key role later in maintain dispatching and ramping continuity for generator units or storage capability of the EVs, respectively.

(v) The other important property of the BP operator that is used to represent objective function, which is presented by:

$$\int_{t_m}^{t_{m+1}} \Re_{Q_m}^{x_t} = \int_{t_m}^{t_{m+1}} \left(\vec{C}_{Q_m}^{x_t} \cdot \vec{B}_{q,Q}^{t} \right) dt = \frac{\sum_{q_m}^{Q_m} C_{q_m}^{x_t}}{Q_m + 1} \tag{4j}$$

The following section presents, the continuous-time model of electric power and natural gas constraints base on the BP operator have been presented.

A. Wind Power, Electricity Load and Non-Electricity Load Profiles: The electricity load, non-electricity load and wind power profiles are main components in both energy systems, i.e., power and natural gas systems, and plays key roles in co-operation of both energy systems. Thus, in this section, these profiles have been modelled based on continuous-time model. Noted that, these profiles are similar in continuous-time model. Therefore, three profiles can be represented by the vector of the BP operator of degree Q as follows:

$$\Phi_{Q_m}^{\Omega} = \vec{C}_{Q_m}^{\Omega} \vec{B}_{q_m,Q_m}^{t-t_m}, \quad \forall t \in [t_m, t_{m+1}), \Omega \in \left\{ P_{s,wt}, P_{nt}, L_{it}^{n} \right\} \tag{5a}$$

where $\vec{C}_{Q_m}^{\Omega}$ is vector of Bernstein coefficients that each element of this vector is weighted by the values of wind power, electricity load and non-electricity load at hour t_m and sub-hour q_m, similar to Fig.1.

B. Inequality Constraints:

The major constraints in both energy system models include inequality constraints like constraints (5).

$$a^{\min} \le x_t \le a^{\max} \tag{5b}$$

$$b^{\min} \le y_t \le b^{\max} \tag{5c}$$

$$A \cdot x_t \le B \cdot y_t \tag{5d}$$

$$\dot{a}^{\min} \le \dot{x}_t \le \dot{a}^{\max} \tag{5e}$$

Constraints (5b) and (5c) mimic (2a), (2h), (2i), (2k), (2o), (2p), (2s), (3b), (3d), (3g), (3j), and (3l) – (3n) that define the limitation on decision variables.

The inequality constraints (5b) and (5c) can be represented in the continuous-time model by the BP operator as follows:

$$\Omega_1^{\min} \le \Phi_{Q_m}^{\Omega_2} = \vec{C}_{Q_m}^{\Omega_2} \vec{B}_{q_m,Q_m}^{t-t_m} \le \Omega_1^{\max}, \quad \forall t \in [t_m, t_{m+1}) \quad \Omega_1^{\min/\max} \in \left\{ a^{\min/\max}, b^{\min/\max} \right\}, \Omega_2 \in \left\{ x_t, y_t \right\} \tag{5f}$$

In (5f), $\vec{C}_{Q_m}^{\Omega_2}$ is vector of Bernstein coefficients of $\Omega_2 \in \left\{ x_t, y_t \right\}$. According to (4f), the $\Phi_{Q_m}^{\Omega_2}$ is limited between max and min Bernstein coefficients, i.e., $\Omega_1^{\min/\max}$.

Likewise, the continuous-time model of inequality constraint (5d) has been presented by (5g):

$$A\cdot\left(\vec{C}_{Q_m}^{x_t}\vec{B}_{Q_m}^{t-t_m}\right)\le B\cdot\left(\vec{C}_{Q_m}^{y_t}\vec{B}_{Q_m}^{t-t_m}\right),\quad \forall t\in[t_m,t_{m+1}) \tag{5g}$$

Noted that, the $\vec{B}_{Q_m}^{t-t_m}$ can be removed from both sides of the constraint (5g), so, this constraint is written as follows:

$$A\cdot\left(\vec{C}_{Q_m}^{x_t}\right)\le B\cdot\left(\vec{C}_{Q_m}^{y_t}\right),\quad \forall t\in[t_m,t_{m+1}) \tag{5h}$$

where $\vec{C}_{Q_m}^{x_t}$ and $\vec{C}_{Q_m}^{y_t}$ are vectors of Bernstein coefficients of x_t and y_t, respectively. *A* and *B*, are suitable matrices. The continuous-time model of constraint (5d) is like (3j) and (3h).

Similarly, constraint (5d) mimic (2b), (2q), (2r), (3o) and (3p) that continuous-time model of this constraint has been presented by:

$$\underline{a}'\le\dot{\Phi}_{(Q-1)_m}^{x_t}=Q_m\vec{C}_{(Q-1)_m}^{\dot{x}_t}\vec{B}_{(Q-1)_m}^{t-t_m}\le\overline{a}' \tag{5i}$$

$$\vec{C}_{(Q-1)_m}^{\dot{x}_t}=Q_m\left[C_{1_m,(Q-1)_m}^{\dot{x}_t}-C_{0_m,(Q-1)_m}^{\dot{x}_t},\cdots,C_{(Q-1)_m,(Q-1)_m}^{\dot{x}_t}-C_{(Q-2)_m,(Q-1)_m}^{\dot{x}_t}\right] \tag{5j}$$

According to (4g), the constraint (5i) can be written as follows:

$$\frac{\underline{a}'}{Q_m}\le\vec{C}_{(Q-1)_m}^{\dot{x}_t}\le\frac{\overline{a}'}{Q_m} \tag{5k}$$

B. Equality Constraints:

$$F\cdot x_t+G\cdot y_t=E\cdot\Omega_t \tag{5l}$$

$$H\cdot\frac{dx_t}{dt}=J\cdot y_t-K\cdot z_t \tag{5m}$$

Constraints (5l) is like constraints (2f), (2g), (2j), (2m), (3c), (3e), (3q), (3r) and (3s). By replacing the Bernstein models of x_t, y_t and Ω_t $\left\{\Phi_{Q_m}^{x_t}=\vec{C}_{Q_m}^{x_t}\vec{B}_{Q_m}^{t-t_m},\Phi_{Q_m}^{y_t}=\vec{C}_{Q_m}^{y_t}\vec{B}_{Q_m}^{t-t_m},\Phi_{Q_m}^{\Omega_t}=\vec{C}_{Q_m}^{\Omega_t}\vec{B}_{Q_m}^{t-t_m}\right\}$ in equality constraint (5l) we have:

$$F\cdot\left(\vec{C}_{Q_m}^{x_t}\vec{B}_{Q_m}^{t-t_m}\right)+G\cdot\left(\vec{C}_{Q_m}^{y_t}\vec{B}_{Q_m}^{t-t_m}\right)=E\cdot\left(\vec{C}_{Q_m}^{\Omega_t}\vec{B}_{Q_m}^{t-t_m}\right) \tag{5n}$$

Then, by removing $\vec{B}_{Q_m}^{t-t_m}$ from both side equality constraint (5l), constraint (5o) is obtained:

$$F\cdot\vec{C}_{Q_m}^{x_t}+G\cdot\vec{C}_{Q_m}^{y_t}=E\cdot\vec{C}_{Q_m}^{\Omega_t} \tag{5o}$$

Similarly, by substituting the Bernstein models of x_t, y_t and z_t, i.e., $\left\{\Phi_{Q_m}^{x_t}=\vec{C}_{Q_m}^{x_t}\vec{B}_{Q_m}^{t-t_m},\Phi_{Q_m}^{y_t}=\vec{C}_{Q_m}^{y_t}\vec{B}_{Q_m}^{t-t_m},\Phi_{Q_m}^{z_t}=\vec{C}_{Q_m}^{z_t}\vec{B}_{Q_m}^{t-t_m}\right\}$ in (5m) and integrating constraint (5m) from t_{m-1} to t_m, this constraint can be written as follows:

$$H\int_{t_{m-1}}^{t_m}\frac{d\Phi_{Q_m}^{x_t}}{dt}=\int_{t_{m-1}}^{t_m}\left(J\cdot\Phi_{Q_m}^{y_t}-K\cdot\Phi_{Q_m}^{z_t}\right)=H\cdot\left(\vec{C}_{(Q+1)_m}^{x_{t_m}}\vec{B}_{(Q+1)_m}^{t-t_m}-\vec{C}_{(Q+1)_m}^{x_{t_{m-1}}}\vec{B}_{(Q+1)_m}^{t-t_m}\right)=\left(J\cdot\left(\vec{C}_{(Q+1)_m}^{y_{t_m}}\vec{B}_{(Q+1)_m}^{t-t_m}\right)-K\cdot\left(\vec{C}_{(Q+1)_m}^{z_{t_m}}\vec{B}_{(Q+1)_m}^{t-t_m}\right)\right) \tag{5p}$$

By removing $\vec{B}_{(Q_m+1)}^{t-t_m}$ from both sides of the equation (5p), we have:

$$H\cdot\left(\vec{C}_{(Q+1)_m}^{x_{t_m}}-\vec{C}_{(Q+1)_m}^{x_{t_{m-1}}}\right)=\left(J\cdot\vec{C}_{(Q+1)_m}^{y_{t_m}}-K\cdot\vec{C}_{(Q+1)_m}^{z_{t_m}}\right) \tag{5q}$$

Noted that, *H, J* and *K*, are constant coefficient matrices. Likewise, constraints (5m) is like constraints (2l) and (3k).

C. Integral equations:

$$\int_{T}\left(A\cdot x_t + B.y_t\right)dt \tag{5r}$$

According to (4j), the objective (1) and constraint (2n) can be converted to (5s).

$$\frac{\sum_{q_m}^{Q_m}\left(A\cdot C_{q_m}^{x_t} + B\cdot C_{q_m}^{y_t}\right)}{Q_m+1} \tag{5s}$$

where *A* and *B*, are suitable matrices.

Equation (5r) is like the objective (1) and constraint (2n).

5. Simulation results

In this section, to demonstrate the effectiveness of the stochastic co-operation of both energy systems with EVs, the 24-bus IEEE RTS system [32] with a 10-node natural gas system has been used, which are shown in Figs.2 and 3. As can be seen from Fig.2, the 24-bus IEEE RTS system comprises 5 GFGUs (red color), 21 fossil units (blue color), 2 wind farms, 17 load buses, 38 transmission lines and one stationary for EV fleet at bus 3. From the Fig.2 it can be seen that the wind farms with the 250 MW and 800 MW capacities have been installed at buses 7 and 9, respectively. Fig.3 shows the ten-node natural gas system, which has 10 pipelines, 2 compressors, 2 natural gas storage (NGS), 8 natural gas loads and 3 suppliers. This figure shows that G9-11, G21 and G23 are GFGUs which are supplied by natural gas nodes 4, 7, and 10, respectively. Other detailed natural gas system parameters are specified in Appendix section. Furthermore, in the modified RTS system a stationary EVs at bus 3 vehicles has been considered. The maximum number of available EVs at bus 3 is 6000 vehicles which is different in each hour. Fig.3. (a) shows the number of available EVs at bus 3 for each hour in per unit [p.u.]. The charge/discharge power, max/min storage capacity, price and charge efficiency for 6000 EVs are shown in Table 2. Noted that, λ_e value in Table 2 shows the percentage of 6000 EVs that are operating as an energy storage device or the EVs participation factor, also, this value can change between 0 and 1. Fig. 4 (b)-(d) shows the electricity load, wind power and natural gas load profiles for CTM and HDTM, respectively. Noted that, since the number of EVs in transmission level is very large, so, the profile of number of EVs can indicate in continuous time curve. In this study, 10 scenarios as input data have been used to show performance of proposed model. Furthermore, in this work, the GFGUs and EVs have been considered as fast response resources due to the fact that they have fast response capabilities such as fast-start and fast-ramping capabilities. Also, the number of variables and equations and solution time for the proposed CTM and HDTM models are presented in the Table 3. The proposed problem formulation has been modelled by GAMS software and implemented on a PC with Intel Core-i7 processor at 4.2 GHz and 16 GB of RAM.

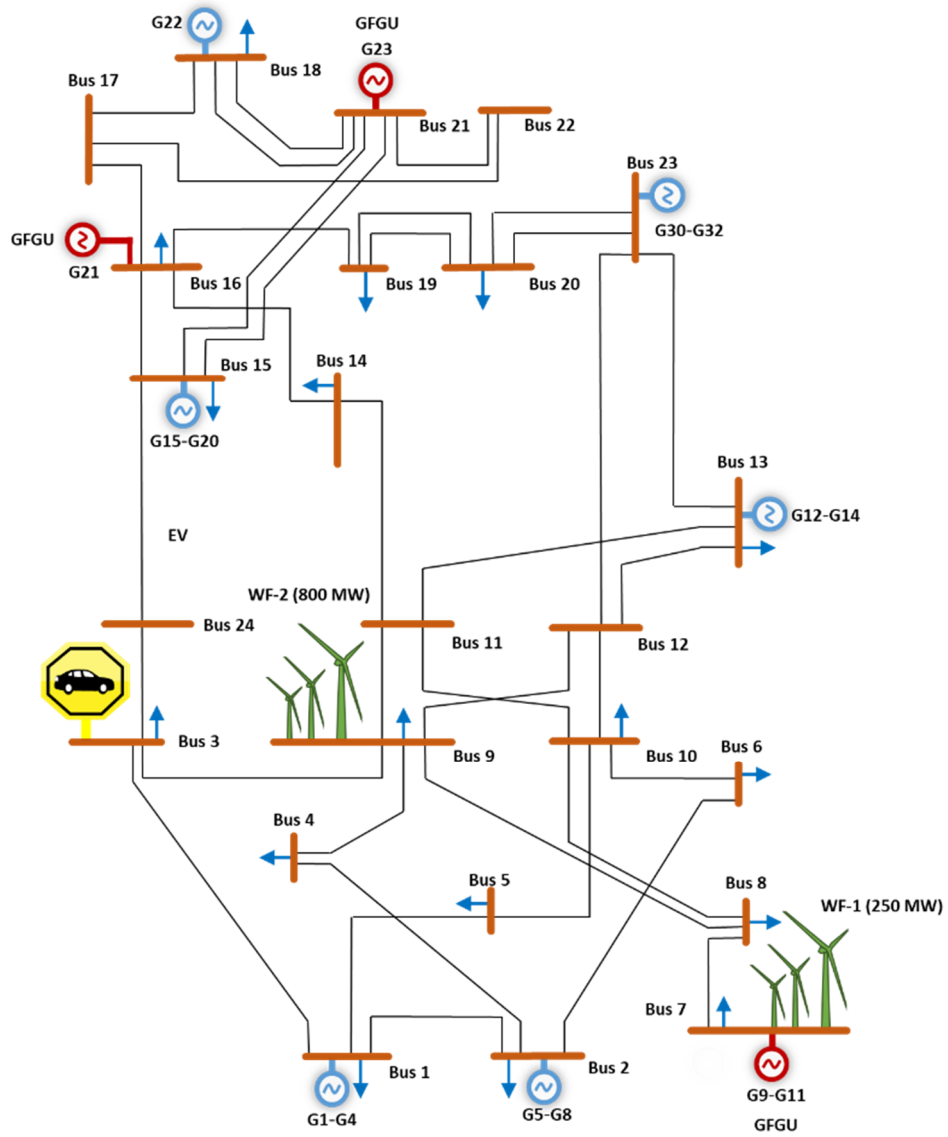

Fig. 2. *Modified IEEE-RTS.*

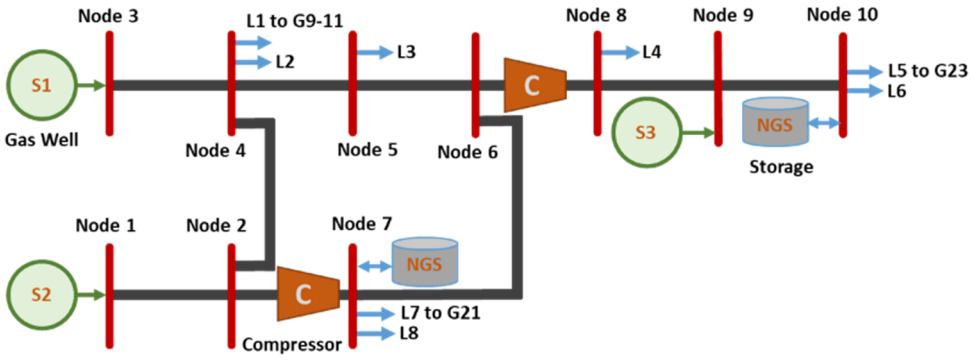

Fig. 3. *Ten-node NGS.*

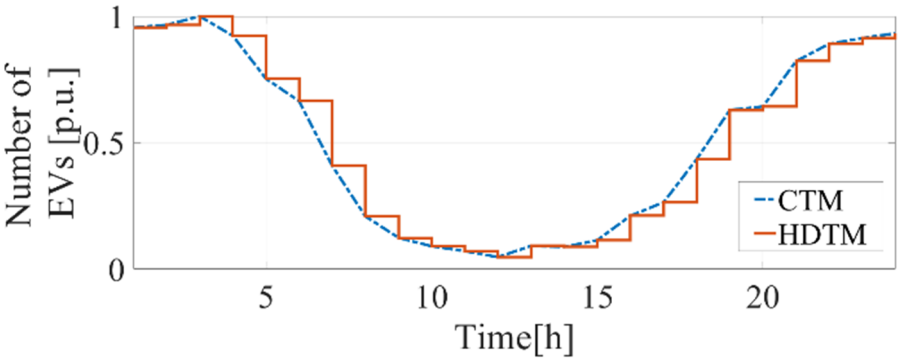

(a)

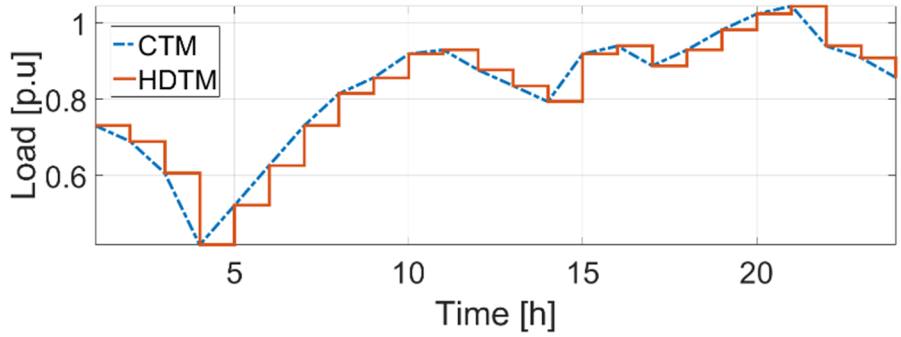

(b)

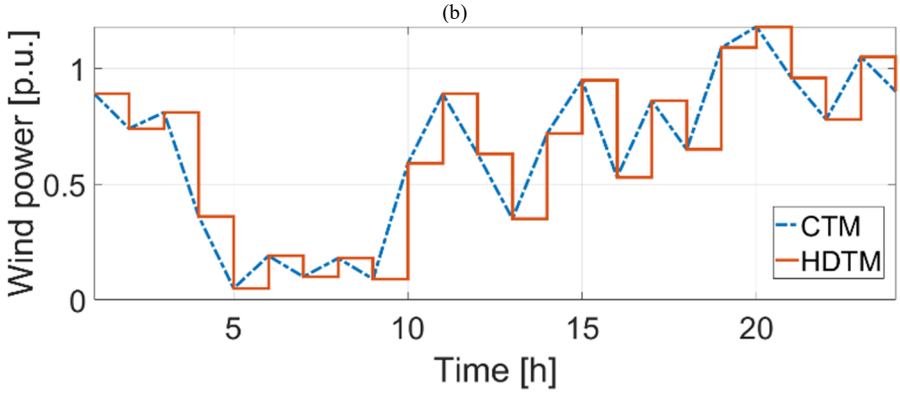

(c)

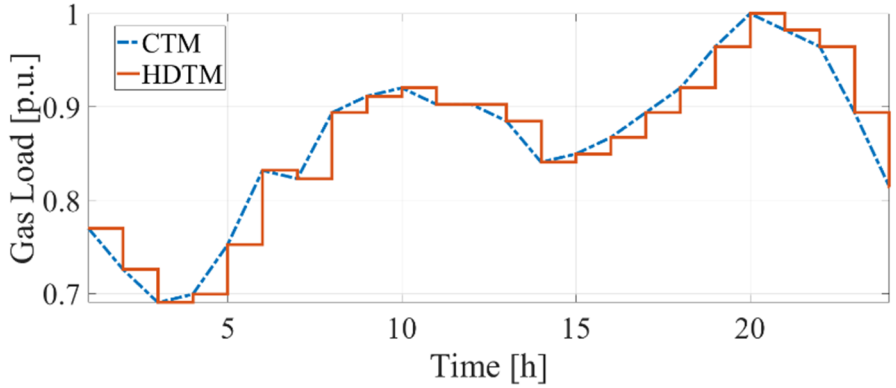

(d)

Fig. 4. (a). *The number of EVs,* (b) *the electricity load,* (c) *the wind power generation,* (d) *the actual gas load curves for CTM and HDTM in* [*p.u.*].

Table 2: Characteristics of stationary EVs.

Number of EV	Min cap. (MWh)	Max cap. (MWh)	Min charge/ dischage (MWh)	Max charge/ discharge (MWh)	Price ($/MW)	η^c / η^d (%)
$6000\lambda_e$	$5\lambda_e$	$100\lambda_e$	$1\ \lambda_e$/ $1\lambda_e$	$80\ \lambda_e$/ $80\lambda_e$	9.20	98

Table 3: Summary of the proposed problem size and its run-time for CTM and HDTM.

Model	Variables		Constraints		Run-time [min]
	Continuous	Binary variables	Equality	Inequality	
HDTM	16804	624	36110	72342	1
CTM	50462	624	108331	205345	4

In this study, two cases have been studied to demonstrate performance of proposed model:

***Case* 1:** Only the GFGUs, without (with) the NGSSCs, are considered as fast-response resource.

***Case* 2:** The both fast-response resources, i.e., the GFGUs and EVs, have been considered.

In this section, two different cases for CTM and HDTM are simulated and compared to analyse the solution results. It should be noted that, for each case, the solution results which have been obtained by CTM and HDTM compare.

These cases are discussed as follows:

***Case* 1:** In this case, the battery of EV are operating only as load (or only charging mode), i.e., λ_e value is 0. The power charging in each hour indicates in Fig.4 (a). Accordingly, the fast response capability is provided only by GFGUs, to follow fast variations of WEGs. The hourly unit commitment (UC) statuses of the inexpensive GFGUs for HDTM/CTM without and with NGSSCs are shown in Tables 4 and 5, respectively. It is apparent from these tables that units G21 and G23 without (with) the NGSSCs are committed at all (or certain) hours to cover the uncertainty of WEG at bus 9, while the units G9-G11 are committed at certain hours to provide enough up/down ramping capabilities for handling uncertainty of WEG at bus 7. What is interesting about the data in Table 5 is that the introduction of NGSSCs into the power system scheduling would reduce hourly commitment of GFGUs because of gas shortages. This fact has been revealed in Table 6, as shown in this table, the introduction of NGSSCs into the power system scheduling has reduced the daily gas consumption of GFGUs at both time models, i.e., CTM and HDTM. This gas shortages (or reduction in gas consumption) is expected, because the natural gas is preferentially scheduled to supply the higher-priority residential natural gas loads with uninterrupted natural gas contract service.

From the data in Fig. 4. (c), it is apparent that wind power generation and power variation are relatively high in hours 11–24 where the power system with the NGSSCs cannot provide enough up/down ramping capabilities to effectively utilizing available wind energy. On the other hand, in these hours where electrical load and natural gas load are relatively high, in this condition, the GFGUs cannot be committed to generate electricity and sustain power balance by providing up/down ramping capabilities to handle wind power variability and uncertainty. All things considered, the NGSSCs will further impact ramp provisions.

In order to cope with natural gas shortages and provide ramp capacity in power system, two primary options are commonly utilized: committed more expensive coal units and/or WEC. Commitment of more coal units may solve natural gas shortages problem but it causes that the TEC increases, thus, which is supposed to be an expensive option here. Nevertheless, wind farm can cope with natural gas and ramp shortages from its curtailment, so, this option would be the more economic option than first option.

Closer inspection of Table 7 shows the largest WEC value occurs when the NGSSCs are considered in power system scheduling, likewise, it can be seen from the data in Table 8 that the TEC has highest value for the CTM and HDTM. What is interesting about the data in Tables 4-7 is that time model is an important component in the scheduling problem, and plays a key role in save scheduling cost and wind energy utilization.

On the other hand, the fast ramping capability is a fundamental property of the GFGUs and battery of EVs that need to a suitable time model. The main disadvantage of conventional HDTM is that the sub-hourly variation of WEG or load could not handle with this model. Accordingly, the actual performance of the GFGUs and EVs with fast-response capabilities is limited by conventional HDTM. When comparing CTM results to conventional HDTM results, it must be pointed out that CTM can play an important role in obtained results. It is apparent from Table 4-5 that more GFGUs are readily online in response to frequent sub-hourly variation of WEG, which is ignored in conventional HDTM.

Accordingly, from the results in Table 6, it is clear that natural gas consumption of GFGUs in CTM is more than conventional HDTM. There are several possible explanations for this result. The prime cause of the higher natural gas consumption in CTM is due to in this model more energy needs to generate energy.

Interestingly, as shown in Table 8, with increasing natural gas consumption of GFGUs in CTM, the TEC in this model is lower than the TEC in conventional HDTM. Two main reasons emerged from this result. First in CTM wider range of wind energy variability and uncertainty could be covered, second, the WEC in the CTM is reduced, which has been indicated by Table 7. For example, as can be seen from the Tables 6-7, the WEC, for α=0 and without NGSSCs, about to 9.4% is reduced by the CTM and also the CTM provide 9.8% cost saving for power system operator as compared to HDTM.

***Case* 2:** In this case, the EVs as an energy storage system is introduced at bus 3 to analyse its impact on the power system scheduling without (with) the NGSSCs. In this study, the EVs participation factor, i.e., λ_e value, is varied from 0 to 0.5. As can be seen in Tables 7 and 8, with increasing the storage capacity, i.e., λ_e value from 0 to 0.5, the TEC and the WEC are decreased. It is probable that the reason for these results is that energy storage capability of EVs increase the penetration level of WEG by reducing the wind curtailment, thus, this action could reduce the hourly commitment of expensive units and reduce the system operation cost.

Table 4: Hourly commitment status of GFGUs for HDTM/CTM without NGSSCs.

Unit\hour		1	2	3	4	5	6	7	8	9	10	11	12	13	14	15	16	17	18	19	20	21	22	23	24
HDTM	G9	**0**	1	0	**1**	1	1	1	1	1	1	1	1	1	1	1	1	1	1	0	**0**	1	1	**1**	**0**
	G10	0	**1**	0	**1**	1	1	1	1	1	1	1	1	1	1	1	1	0	1	1	1	1	1	**0**	1
	G11	0	1	0	1	1	1	1	1	1	1	1	1	1	1	1	1	1	1	**1**	**1**	1	1	**0**	**0**
	G21	1	1	1	1	1	1	1	1	1	1	1	1	1	1	1	1	1	1	1	1	1	1	1	1
	G23	1	1	1	1	1	1	1	1	1	1	1	1	1	1	1	1	1	1	1	1	1	1	1	1
CTM	G9	0	0	0	**1**	1	1	1	1	1	1	1	1	1	1	1	1	1	1	1	1	1	1	1	1
	G10	0	0	0	1	1	1	1	1	1	1	1	1	1	1	1	1	1	1	1	1	1	1	1	1
	G11	0	0	0	**0**	1	1	1	1	1	1	1	1	1	1	1	1	1	1	1	1	1	1	1	1
	G21	**1**	**1**	**1**	1	1	1	1	1	1	1	1	1	1	1	1	1	1	1	1	1	1	1	1	1
	G23	1	1	1	1	1	1	1	1	1	1	1	1	1	1	1	1	1	1	1	1	1	1	1	1

Table 5: Hourly commitment status of GFGUs for HDTM/CTM with NGSSCs.

Unit\hour		1	2	3	4	5	6	7	8	9	10	11	12	13	14	15	16	17	18	19	20	21	22	23	24
HDTM	G9	0	1	0	0	0	0	0	0	0	**0**	1	**1**	**0**	**0**	0	**0**	1	0	**0**	**0**	**1**	1	**0**	**0**
	G10	0	**0**	**0**	**1**	0	**1**	0	**0**	**1**	0	**1**	0	0	0	**1**	**0**	1	1	**1**	**0**	**1**	0	0	0
	G11	**0**	**0**	0	0	0	0	0	**0**	0	**0**	**0**	0	**0**	1	1	**0**	1	0	0	1	1	0	0	0
	G21	1	**1**	1	**0**	1	**0**	1	1	1	1	1	1	**1**	1	1	**1**	0	1	1	1	1	1	**1**	**1**
	G23	**1**	0	**1**	0	**1**	**0**	1	1	1	**1**	0	**0**	**1**	0	**0**	**1**	**0**	1	1	1	1	1	1	1
CTM	G9	0	0	0	0	0	0	0	**0**	1	1	1	1	1	1	1	1	1	1	1	1	1	1	1	1
	G10	**1**	**1**	**1**	**1**	**1**	**1**	**1**	1	1	1	1	1	1	1	1	1	1	1	1	1	1	1	1	1
	G11	0	0	0	0	0	0	**0**	1	1	1	1	1	1	1	1	1	1	1	1	1	1	1	1	1
	G21	0	0	0	0	1	1	1	1	1	1	1	1	1	1	1	1	1	1	1	1	1	1	1	1
	G23	1	1	1	1	1	1	1	1	1	1	1	1	1	1	1	1	1	1	1	1	1	1	1	1

Interestingly, from the data in Table 6 without NGSSCs, it is apparent that with increase λ_e value the natural gas consumption of GFGUs in HDTM increases, but, in CTM reduces. These results are likely, utilization of energy storage capability of EVs with CTM more modifies the schedule of GFGUs compared to HDTM. What is interesting about the data in this table is that for same λ_e value the natural gas consumption of GFGUs with the NGSSCs in CTM increases, but, in HDTM decreases. Nevertheless, closer inspection of the Tables 6 and 8 show that while the natural gas consumption in CTM is increased, the TEC is reduced. The main possible reason for this result is that the WEG uncertainty in CTM is more covered than HDTM, as can be seen in Table 7, the WEC for CTM is more reduced than HDTM.

In order to better understanding, the results of energy storage in EVs battery in CTM and HDTM, for λ_e = 0.25 and 0.50, are compared in Tables 4 and 5 and Figs. 5 (a) and (b).

Noted that, the changes in the hourly GFGUs states for λ_e = 50 compared to λ_e = 0, are highlighted in Tables 4 and 5. As shown in Tables 3 and 4, the energy storage capability of EVs in CTM more reduces hourly commitment of the GFGUs in scheduling horizon than HDTM.

Similarly, Figs. 5 (a) and (b) indicate the EVs energy storage at each hour. What is interesting about the data in these figures is that with a higher λ_e value in CTM, the energy storage profile will be increasingly close to the WEG profile, which is neglected by HDTM. In an extreme case, once λ_e = 0.50 in CTM, the energy storage profile would almost match that of WEG profile in which the variation of WEG is covered by energy storage in EVs. Consequently, it is concluded that the CTM has a great capability to utilize more storage capacity of EVs, and also, it can more mitigate the variability of WEG than HDTM.

Computation Burden*:* The number of binary variables is the same for both the CTM and HDTM. In the CTM, continuous variables and equality/inequality equations are represented in more than HDTM in each hour. Consequently, it is predictable that the computation time and memory consumption is higher for the CTM. Point often overlooked, as this is an offline practice which is performed in the prior day, execution time is not of utmost importance. Model statistics are presented in Table 3. The CPU time needed to solve the CTM for a 24-bus system is about to 4 min, which is reasonable for a PC with Intel Core-i7 processor at 4.2 GHz and 16 GB of RAM. However, to implement the CTM in a real-time system with thousands of nodes and lines, the following additional alternatives are also available:

- To use a supercomputer,
- To implement parallelization techniques [28],
- To apply appropriate techniques to simplify the network [28],
- To decompose the transmission system by area [28].

Discussion: This paper proposes a new model for co-operation of electric power system with natural gas system in discrete-time and continues-time frameworks, while considering the fast-response resources, i.e., the GFGUs and EVs, to handle uncertainty of WEG.

As mentioned previously, the main aims of paper address the following questions:

(i) Would influence natural gas system security constraints on gas consumption, wind energy curtailment and electrical generation cost?

As expected, the obtained results in this study responded to this question. All GFGUs were most dispatched in electrical power system operation because their generation costs are inexpensive and they have the highest ramping capability. Fossil units are placed at the second since they are the most expensive and have low ramping capability. Also, for electrical power systems integrated with large-scale WEG, significant amounts of WEG cannot be absorbed due to low ramping capability. Accordingly, the GFGUs can play an important role in enhance ramping capacity and absorbing WEG and reduce WEC. Nevertheless, once

natural gas system security constraints are incorporated for five GFGUs the fuel consumptions of five cheapest GFGUs is reduced since natural gas system security constraints have limited the supply of fuel. For this reason, the outputs of the five cheapest GFGUs are decreased and enforce the expensive fossil units to be committed. Consequently, the generation cost for electrical system is increased.

(ii) Would influence integration of EVs in electric power system on the natural gas system operation?

A satisfactory response to this question may be that the scarcity of ramping capacity is the main obstacle to decrease the commitment of GFGUs. Accordingly, in these results, if there was no EVs in the joint scheduling system, the system would partially overcome this scarcity by increasing share of GFGUs in generation.

Similarly, if there was the EVs in the joint scheduling system, the system could overcome this scarcity by ramping capability of flexible EV batteries. In this condition, the share of GFGUs in generation is reduced which is caused to decrease the natural gas consumption.

(ii) Would influence time model on the co-scheduling of the integrated electric energy and natural gas systems with GFGUs and EVs?

The overall response to this question was surprisingly.

Using the simulations conducted on the IEEE-RTS, it was observed that the proposed continues-time framework provides a continuous-time schedule for GFGUs and EVs which more efficiently utilizes their ramping capability to follow the continuous-time variations of the WEG and load than discrete-time framework. Accordingly, the obtained results reveal that the proposed continues-time framework as compare to the discrete-time framework, provides more decrease in the gas consumption, WEC and TEC values.

Table 6: Gas consumption of GFGUs [kcf] for HDTM and CTM without (with) NGSSCs under different α value.

α	Without NGSSCs		With NGSSCs	
	HDTM	CTM	HDTM	CTM
0.00	145.12	151.15	122.88	131.81
0.25	153.21	149.81	122.88	131.23
0.50	154.28	146.87	122.88	131.43

Table 7: The WEC [MWh] for HDTM and CTM without (with) NGSSCs under different α value.

α	Without NGSSCs		With NGSSCs	
	HDTM	CTM	HDTM	CTM
0.00	274.76	248.71	306.3	302.12
0.25	128.14	98.91	132.455	102.42
0.50	57.042	43.12	61.16	43.83

Table 8: The TEC [M$] for DTM and CTM without (with) NGSSCs under different α value.

α	Without NGSSCs		With NGSSCs	
	HDTM	CTM	HDTM	CTM
0.00	0.523	0.471	0.590	0.586
0.25	0.476	0.428	0.478	0.448
0.50	0.460	0.437	0.474	0.444

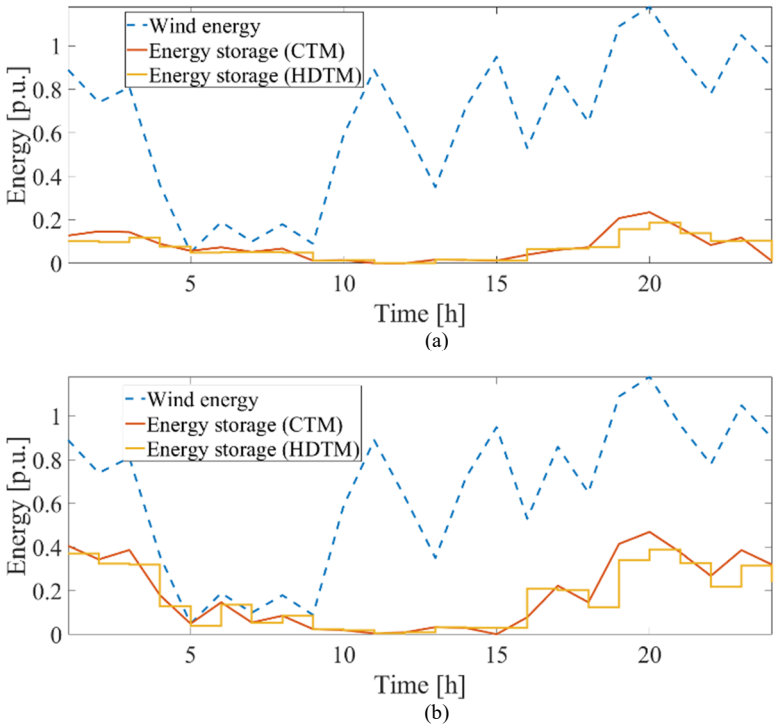

Fig. 5 . *The energy storage in the EVs for CTM and HDTM in [p.u.]; a) α=0.25 and b) α=0.5.*

6. Conclusions

In this paper, the impact of GFGUs and storage capability of EVs as fast-response resources on augmenting integration of WEG is evaluated. This paper proposes a two-stage stochastic model for co-operation of electric power system with natural gas system, with a full model NGSSCs, in continuous-time framework, while considering uncertainty of WEG. This paper seeks to address the following questions: (i) how EVs can reduce effect of the NGSSCs on power system operation and provide ramp capacity to accommodate the variable wind energy; (ii) whether continuous-time framework can have a positive effect on co-operation of electric power and natural gas systems and reduce WEC. To answer above questions, at first, the two-stage continuous-time stochastic co-operation of electric power with natural gas systems model has been implemented on the IEEE-RTS. The obtained results highlighted that the EVs with energy storage and fast ramp capabilities can compensate shortage of GFGUs in scheduling problem and reduce effect of NGSSCs on power system operation. Also, the results confirm the usefulness of CTM as a time framework to more utilize high ramping capability of fast-response resources to follow the continuous-time variations of the WEG than discrete-time framework. Therefore, the obtained results reveal that the proposed continuous-time framework as compare to the discrete-time framework, provides more decrease in the TEC, natural gas consumption (in same case) and EWEC values.

7. Future works

Previous sections showed the effectiveness of coordination of the electricity and natural gas systems can enhance integration of large-scale WEG and EV batteries in power systems. Even though the results are hopeful, the further studies would be

necessary to confirm the effectiveness of electricity and natural gas systems the method under more realistic set of assumptions:

AC feasibility: AC feasibility of electricity system adjustments should be studied and confirmed before the solution can be implemented. In order to do that, further research is needed to include an AC model to check the solutions coming out of a DCOPF.

Stability: the dynamic stability analysed for interaction of the electricity and natural gas systems can be studied.

Uncertainty of EVs: Further research is required to determine whether **uncertainty** of EV have effect on interaction of the electricity and natural gas systems or not.

8. Acknowledgment

J.P.S. Catalão acknowledges the support by FEDER funds through COMPETE 2020 and by Portuguese funds through FCT, under POCI-01-0145-FEDER-029803 (02/SAICT/2017).

Appendix

This Appendix provides parameters of gas transmission system in Table 9–13.

Table 9: Parameters of nodes in a gas transmission system.

Node No.	Min-Pressure (Psig)	Max-Pressure (Psig)
1	***350***	***370***
2	310	330
3	***350***	***370***
4	290	310
5	240	260
6	270	290
7	250	270
8	310	330
9	***350***	***370***
10	270	290

Table 10: Parameters of pipelines in a gas transmission system.

Index	From Node	To Node	π (kcf/Psig)
Pipe 1	9	10	20
Pipe 2	8	6	20
Pipe 3	9	8	20
Pipe 4	7	6	15
Pipe 5	6	5	15
Pipe 6	2	7	15
Pipe 7	2	4	15
Pipe 8	4	5	20
Pipe 9	3	4	20
Pipe 10	1	2	20

Table 11: Parameters of a natural gas supplier.

Supplier No.	Node No.	$\underline{G}_i$ (kcf/h)	$\overline{G}_i$ (kcf/h)
1	1	1000	6000
2	3	1500	6000
3	9	1500	15000

Table 12: Parameters of gas load

Load No.	Node No.	Gas amount (kcf)	Priority
1	4	Determined by G9	medium
1	4	Determined by G10	medium
1	4	Determined by G11	medium
2	4	Residential 1000	high
3	5	Residential 1700	high
4	8	Residential 1200	high
5	10	Determined by G23	medium
6	10	Residential 1300	high
7	4	Determined by G21	high
8	7	Residential 1000	high

Table 13: Parameters of gas storage.

Name	$\underline{\Psi}_i^{\max}$	$\overline{\Psi}_i^{\max}$	Φ	Φ^{in}
NGS1	300	300	600	300
NGS2	150	150	300	150

References

[1] EIA. (2014 Apr.). Annual Energy Outlook 2014 With Projections to 2040 [Online]. Available: http://www.eia.gov.

[2] M. Shahidehpour, Y. Fu, and T. Wiedman, "Impact of natural gas infrastructure on electric power systems," *Proceedings of the IEEE,* vol. 93, no. 5, pp. 1042-1056, 2005.

[3] X. Zhang, L. Che, M. Shahidehpour, A. Alabdulwahab, and A. Abusorrah, "Electricity-natural gas operation planning with hourly demand response for deployment of flexible ramp," *IEEE Transactions on Sustainable Energy,* vol. 7, no. 3, pp. 996-1004, 2016.

[4] X. Zhang, M. Shahidehpour, A. Alabdulwahab, and A. Abusorrah, "Hourly electricity demand response in the stochastic day-ahead scheduling of coordinated electricity and natural gas networks," *IEEE Transactions on Power Systems,* vol. 31, no. 1, pp. 592-601, 2016.

[5] C. Shao, X. Wang, X. Wang, C. Du, C. Dang, and S. Liu, "Cooperative dispatch of wind generation and electric vehicles with battery storage capacity constraints in SCUC," *IEEE Transactions on Smart Grid,* vol. 5, no. 5, pp. 2219-2226, 2014.

[6] A. Antenucci and G. Sansavini, "Gas-Constrained Secure Reserve Allocation With Large Renewable Penetration," *IEEE Transactions on Sustainable Energy,* vol. 9, no. 2, pp. 685-694, 2018.

[7] C. He, L. Wu, T. Liu, W. Wei, and C. Wang, "Co-optimization scheduling of interdependent power and gas systems with electricity and gas uncertainties," *Energy,* vol. 159, pp. 1003-1015, 2018.

[8] G. Li, R. Zhang, T. Jiang, H. Chen, L. Bai, and X. Li, "Security-constrained bi-level economic dispatch model for integrated natural gas and electricity systems considering wind power and power-to-gas process," *Applied energy,* vol. 194, pp. 696-704, 2017.

[9] J. Aghaei, A. E. Nezhad, A. Rabiee, and E. Rahimi, "Contribution of plug-in hybrid electric vehicles in power system uncertainty management," *Renewable and Sustainable Energy Reviews,* vol. 59, pp. 450-458, 2016.

[10] H. Wu, M. Shahidehpour, A. Alabdulwahab, and A. Abusorrah, "Thermal generation flexibility with ramping costs and hourly demand response in stochastic security-constrained scheduling of variable energy sources," *IEEE Transactions on Power Systems,* vol. 30, no. 6, pp. 2955-2964, 2015.

[11] G. Haddadian, N. Khalili, M. Khodayar, and M. Shahidehpour, "Optimal coordination of variable renewable resources and electric vehicles as distributed storage for energy sustainability," *Sustainable Energy, Grids and Networks,* vol. 6, pp. 14-24, 2016.

[12] A. Nikoobakht, J. Aghaei, R. Khatami, E. Mahboubi-Moghaddam, and M. Parvania, "Stochastic flexible transmission operation for coordinated integration of plug-in electric vehicles and renewable energy sources," *Applied Energy,* vol. 238, pp. 225-238, 2019.

[13] M. E. Khodayar, L. Wu, and M. Shahidehpour, "Hourly coordination of electric vehicle operation and volatile wind power generation in SCUC," *IEEE Transactions on Smart Grid,* vol. 3, no. 3, pp. 1271-1279, 2012.

[14] C. Liu, J. Wang, A. Botterud, Y. Zhou, and A. Vyas, "Assessment of impacts of PHEV charging patterns on wind-thermal scheduling by stochastic unit commitment," *IEEE Transactions on Smart Grid,* vol. 3, no. 2, pp. 675-683, 2012.

[15] B. Yang *et al.*, "Applications of supercapacitor energy storage systems in microgrid with distributed generators via passive fractional-order sliding-mode control," *Energy,* vol. 187, p. 115905, 2019.

[16] B. Yang, T. Yu, H. Shu, J. Dong, and L. Jiang, "Robust sliding-mode control of wind energy conversion systems for optimal power extraction via nonlinear perturbation observers," *Applied Energy,* vol. 210, pp. 711-723, 2018.

[17] B. Yang *et al.*, "Novel bio-inspired memetic salp swarm algorithm and application to MPPT for PV systems considering partial shading condition," *Journal of cleaner production,* vol. 215, pp. 1203-1222, 2019.

[18] B. Zhao, A. J. Conejo, and R. Sioshansi, "Coordinated expansion planning of natural gas and electric power systems," *IEEE Transactions on Power Systems,* vol. 33, no. 3, pp. 3064-3075, 2017.

[19] Y. He, M. Shahidehpour, Z. Li, C. Guo, and B. Zhu, "Robust constrained operation of integrated electricity-natural gas system considering distributed natural gas storage," *IEEE Transactions on Sustainable Energy,* vol. 9, no. 3, pp. 1061-1071, 2018.

[20] Y. Li, W. Liu, M. Shahidehpour, F. Wen, K. Wang, and Y. Huang, "Optimal Operation Strategy for Integrated Natural Gas Generating Unit and Power-to-Gas Conversion Facilities," *IEEE Transactions on Sustainable Energy,* vol. 9, no. 4, pp. 1870-1879, 2018.

[21] J. Fang, Q. Zeng, X. Ai, Z. Chen, and J. Wen, "Dynamic optimal energy flow in the integrated natural gas and electrical power systems," *IEEE Transactions on Sustainable Energy,* vol. 9, no. 1, pp. 188-198, 2017.

[22] V. Z. Rad, S. A. Torabi, and H. Shakouri, "Joint electricity generation and transmission expansion planning under integrated gas and power system," *Energy,* vol. 167, pp. 523-537, 2019.

[23] Y. Li *et al.*, "Optimal stochastic operation of integrated low-carbon electric power, natural gas, and heat delivery system," *IEEE Transactions on Sustainable Energy,* vol. 9, no. 1, pp. 273-283, 2017.

[24] M. Ghofrani, A. Arabali, M. Etezadi-Amoli, and M. S. Fadali, "Smart scheduling and cost-benefit analysis of grid-enabled electric vehicles for wind power integration," *IEEE Transactions on Smart Grid,* vol. 5, no. 5, pp. 2306-2313, 2014.

[25] A. Nikoobakht, J. Aghaei, T. Niknam, H. Farahmand, and M. Korpås, "Electric vehicle mobility and optimal grid reconfiguration as flexibility tools in wind integrated power systems," *International Journal of Electrical Power & Energy Systems,* vol. 110, pp. 83-94, 2019.

[26] J. Zhao, C. Wan, Z. Xu, and K. P. Wong, "Spinning reserve requirement optimization considering integration of plug-in electric vehicles," *IEEE Transactions on Smart Grid,* vol. 8, no. 4, pp. 2009-2021, 2016.

[27] J. Zhao, C. Wan, Z. Xu, and J. Wang, "Risk-based day-ahead scheduling of electric vehicle aggregator using information gap decision theory," *IEEE Transactions on Smart Grid,* vol. 8, no. 4, pp. 1609-1618, 2015.

[28] B. Yang *et al.*, "Comprehensive overview of meta-heuristic algorithm applications on PV cell parameter identification," *Energy Conversion and Management,* vol. 208, p. 112595, 2020.

[29] A. Alabdulwahab, A. Abusorrah, X. Zhang, and M. Shahidehpour, "Stochastic security-constrained scheduling of coordinated electricity and natural gas infrastructures," *IEEE Systems Journal,* vol. 11, no. 3, pp. 1674-1683, 2017.

[30] P. Dierckx, *Curve and surface fitting with splines*. Oxford University Press, 1995.

[31] P. M. Prenter, *Splines and variational methods*. Courier Corporation, 2008.

[32] R. T. Force, "The IEEE reliability test system-1996," *IEEE Trans. Power Syst,* vol. 14, no. 3, pp. 1010-1020, 1999.